

Domain Generalization for Mammographic Image Analysis via Contrastive Learning

Zheren Li, Zhiming Cui, Lichi Zhang, Sheng Wang, Chenjin Lei, Xi Ouyang, Dongdong Chen, Zixu Zhuang, Xiangyu Zhao, Yajia Gu, Zaiyi Liu, Chunling Liu, Dinggang Shen*, *Fellow, IEEE*, Jie-Zhi Cheng*, *Member, IEEE*

Abstract—Mammographic image analysis is a fundamental problem in the computer-aided diagnosis scheme, which has recently made remarkable progress with the advance of deep learning. However, the construction of a deep learning model requires training data that are large and sufficiently diverse in terms of image style and quality. In particular, the diversity of image style may be majorly attributed to the vendor factor. However, mammogram collection from vendors as many as possible is very expensive and sometimes impractical for laboratory-scale studies. Accordingly, to further augment the generalization capability of deep learning models to various vendors with limited resources, a new contrastive learning scheme is developed. Specifically, the backbone network is firstly trained with a multi-style and multi-view unsupervised self-learning scheme for the embedding of invariant features to various vendor styles. Afterward, the backbone network is then recalibrated to the downstream tasks of mass detection, multi-view mass matching, BI-RADS classification and breast density classification with specific supervised learning. The proposed method is evaluated with mammograms from four vendors and two unseen public datasets. The experimental results suggest that our approach can effectively improve analysis performance on both seen and unseen domains, and outperforms many state-of-the-art (SOTA) generalization methods.

Index Terms—Domain generalization, mammographic image analysis, contrastive learning.

I. INTRODUCTION

This work was supported in part by the Key Research and Development Program of Guangdong Province, China (2021B0101420006).

Zheren Li, Sheng Wang, Dongdong Chen, Zixu Zhuang, Xiangyu Zhao and Lichi Zhang are with the School of Biomedical Engineering, Shanghai Jiao Tong University, Shanghai 200240, China. (e-mail: {lizheren, wsheng, chendongdong, zixuzhuang, xiangyu.zhao, lichizhang}@sjtu.edu.cn).

Zheren Li, Chenjin Lei, Xi Ouyang, Dinggang Shen and Jie-Zhi Cheng are with Shanghai United Imaging Intelligence Co., Ltd., Shanghai 200030, China. (e-mail: lizheren0613@163.com, chenjin.lei@uii-ai.com, demo.ouyang@gmail.com, dinggang.shen@uii-ai.com, jzcheng@ntu.edu.tw).

Zhiming Cui and Dinggang Shen are with the School of Biomedical Engineering, ShanghaiTech University, Shanghai 201210, China. (e-mail: zmcui@cs.hku.hk, dgshen@shanghaitech.edu.cn).

Yajia Gu are with the Department of Radiology, Fudan University Shanghai Cancer Center, 270 Dongan Road, Shanghai 200032, China. (e-mail: cjr.guyajia@vip.163.com).

Zaiyi Liu and Chunling Liu are with the Guangdong Provincial People's Hospital & Guangdong Academy of Medical Sciences, Guangzhou 510080, China. (e-mail: liuchunling@gdph.org.cn).

* Corresponding authors: Dinggang Shen and Jie-Zhi Cheng.

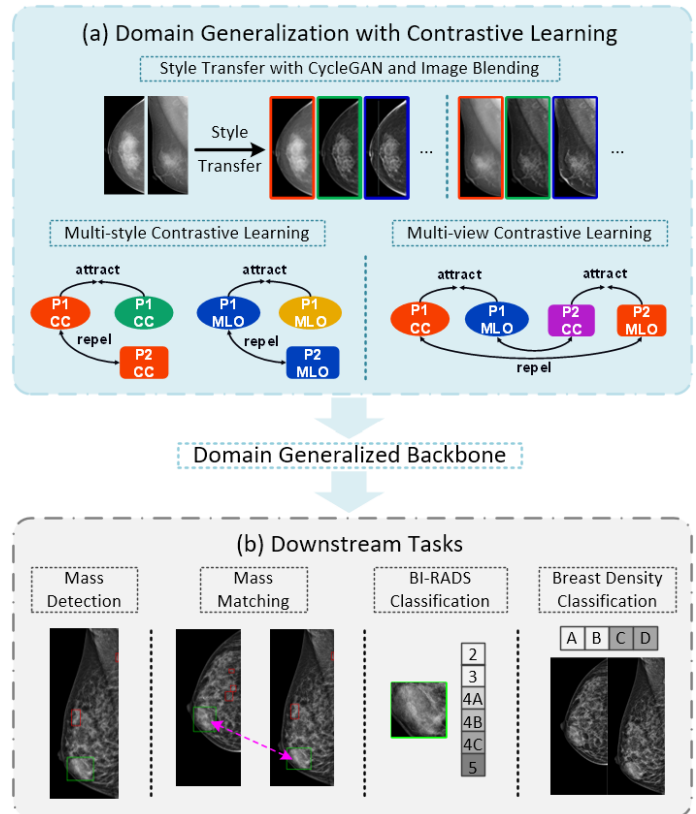


Fig. 1. Our domain generalization method for mammography images involves two main steps. In step (a), we use a combination of CycleGAN and image blending technique to generate diverse vendor styles. This is followed by a multi-style and multi-view contrastive learning approach to extract domain invariant features from unlabeled data obtained from various vendors. In step (b), we transfer the domain generalized backbone to downstream tasks such as mass detection, mass matching, BI-RADS classification, and breast density classification.

BREAST cancer is one of the leading causes of cancer-related deaths among women [1]. Mammography is the conventional imaging technique for early screening of breast cancer. It has been shown in many studies [2]–[4] that advances in deep learning (DL) techniques have remarkably improved the computer-aided detection and diagnosis (CAD) schemes of mammography. The CAD schemes are composed of several components, such as lesion detection [5], lesion matching [6], malignancy classification [7], density classifi-

cation [8], and others. However, most CAD schemes are not well tested for the out-of-distribution generalization, i.e., the applicability to the unseen domains in the training process. Domain shift may result in a significant decline in performance across various vendors [9], [10].

As shown in Fig. I, the styles of images from various vendors vary significantly. The diversity in image style among mammograms from different vendors can be attributed to various factors, like imaging hardware, processing pipeline, etc. With different hardware settings, the following reconstruction and post-processing algorithms may need to be specially tailored and tuned. Therefore, the style of finally generated image can appear very distinctive from vendor to vendor.

These differences in image style pose a significant challenge for CAD systems, particularly those equipped with deep learning. This is because these systems require training data that are diverse and representative of the variability in the real-world. However, it is extremely expensive and impossible to gather vast amounts of diverse data from numerous vendors. Meanwhile, it is also well-known that there exists domain gap between datasets from various hospitals, due to the institutional imaging convention and protocol. Accordingly, the generalization of DL-based CAD systems may be limited if the data of each vendor is not sufficiently included in the training stage. To overcome this challenge, a domain generalization method is needed to alleviate the demands of large and diverse data from various vendors for the DL-based CAD scheme.

The domain generalization for DL technique can be classified into three categories: 1) Conventional data augmentation methods, e.g. rotation, flip, deformation and color jittering [11], [12]. These augmentation methods can help the model to adopt images from slightly different domains. 2) Learning-based methods with the generative deep neural networks which synthesize data in the target domain [13]–[16]. These networks are implemented by learning an image-to-image mapping from the original to the target domain. 3) Learning-based methods for the exploration of task-specific and domain-invariant features [17]–[23]. Instead of learning an image-to-image mapping, these methods directly learned a representation-to-representation mapping. However, all of these learning-based approaches rely on labeled data, which can be expensive to acquire and is often limited in availability. It is crucial to develop a novel approach for automatically extracting domain-invariant features from large, unlabeled datasets.

To address the above-mentioned issues, here we explore the contrastive learning technique to augment the generalization capability of DL-based CAD. Contrastive learning has also been shown to generate better pretrained models for several medical image problems, e.g., diagnosis of chest radiography [24]–[26], dermatology images [24], etc., but is less exploited for extracting domain invariant features. To specifically address the issue of the vendor domain gap, we propose a multi-style and multi-view contrastive learning (MSVCL v2) method to boost the CAD performance in mammography. Specifically, to attain the goal of generalization robustness to multiple vendor styles, the CycleGAN [27] technique is employed to generate multiple vendor-style images from a single vendor-style image. The generated multi-style images from the same

source are randomly paired as positive samples for multi-style contrastive learning (MSCL v2). To further gain generalization capability to the position view, the CC and MLO views of the same breast are also paired as positive samples in the scheme of multi-view contrastive learning (MVCL v2). After self-supervised training, the backbone of the contrastive learning model is employed for the downstream tasks, including mass detection, multi-view mass matching, BI-RADS classification, and breast density classification. For the multi-view mass matching task, we also employ the contrastive learning approach, where the input region of interest (ROI) patches from the CC and MLO views of the same mass are treated as a positive pair.

Our main contributions are summarized in three-fold:

- We propose a novel contrastive learning scheme to improve the model generalization ability in mammographic image analysis tasks. The learning-based scheme roots in contrastive learning, by utilizing multi-style and multi-view for unsupervised representation learning, to enhance the context features extraction that is insensitive to the domain shift.
- We developed four downstream tasks to comprehensively evaluate the generalization ability of mammographic image analysis. These tasks included mass detection, mass matching, BI-RADS classification, and breast density classification.
- We employed a dataset consisting of 27,000 unlabeled images and 2,700 labeled images for our experiments. Our method was trained on three vendor domains and evaluated on both seen and unseen domains from the six-center dataset, which includes two public dataset. The results demonstrated that our method can effectively boost the downstream tasks performance on either seen or unseen domains.

The preliminary version of this work was presented at MICCAI 2021 previously [28]. In this paper, we present an extended version that includes four major improvements. (1) In addition to transferring vendor style from the source domain to the target domain, our style diversification module generates arbitrary combinations of any two vendor styles, which enhances the diversity of vendor styles and helps to better fit the variability of image styles across vendors. (2) We optimize the selection mechanism for positive and negative pairs in contrastive learning based on domain knowledge of mammography. (3) We expand the amount of labeled data by 75%, which includes a larger train/val dataset, and an additional unseen domain test set. Meanwhile, we conduct three additional downstream tasks and ablation studies to evaluate the effectiveness of enhanced multi-style and multi-view contrastive learning. (4) We provide more detailed introductions and elaborated implementation details.

The rest of the paper is organized as follows: Section II gives a brief review of related works. Section III demonstrates the details of the proposed domain generalization method. Experimental results and visualizations are described in Section IV. Finally, Section V concludes the paper and discusses potential future work.

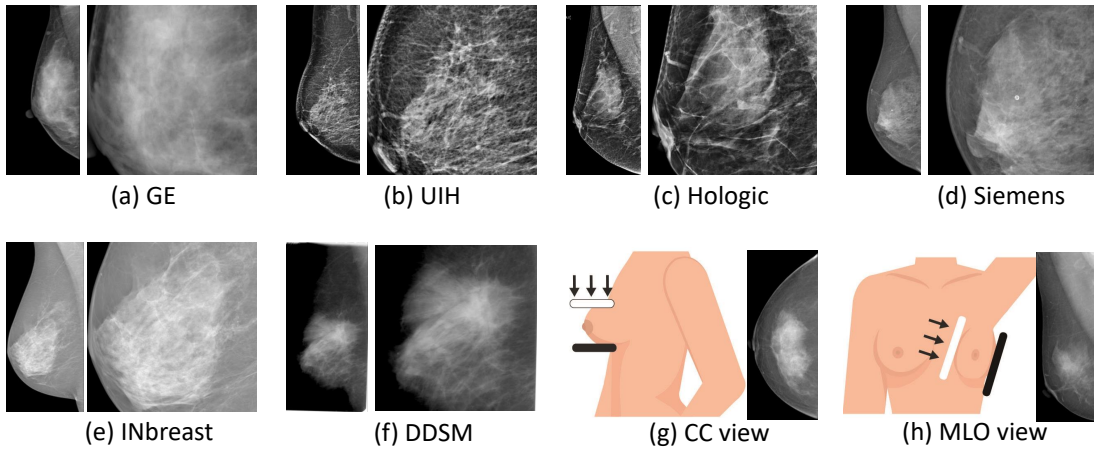


Fig. 2. Style differences among five mammography domains (a-f), i.e., GE, United Imaging Healthcare (UIH), Hologic, Siemens, INbreast and DDSM. All images of the five domains (a-f) are MLO views. To illustrate the detailed image variation, a zoom-in image is provided on the right of each MLO view. Figure (g-h) corresponds to standard projections of CC view and MLO view. The CC view is a top-down view of the breast, whereas the MLO view is a side view taken at a certain angle (usually at an angle of 30–60 degrees) along the chest wall, perpendicular to the long axis of the pectoralis major muscle.

TABLE I

DETAILS OF USAGE FOR THE DATA INVOLVED IN THIS STUDY. SPECIFICALLY, THE COLUMNS "STYLE TRANSFER" AND "SELF-SUPERVISION" SUGGEST THE NUMBER OF IMAGES INVOLVED IN THE TRAINING OF CYCLEGAN AND CONTRASTIVE LEARNING, RESPECTIVELY.

Domain	Dataset	Vendor	Style Transfer	Self-Supervision	Downstream Tasks (train/val/test)
Seen	Style A	GE	1000	8000	600/100/100
	Style B	UIH	1000	8000	600/100/100
	Style C	HOLOGIC	1000	8000	600/100/100
Unseen	Style D	SIEMENS	0	0	0/0/100
	Style E	INbreast	0	0	0/0/100
	Style F	DDSM	0	0	0/0/100

II. RELATED WORKS

A. Domain Generalization

Domain generalization is an important research area to overcome performance degradation caused by cross-domain variations in medical image analysis. Many methods [18], [19], [29]–[31] have been proposed to improve generalization capability through data argumentation or exploiting the general learning strategy. However, learning-based methods are more desirable and related to our work, we focus on this category in the following.

With the recent developments in machine learning techniques, plenty of works utilize representation learning to address the domain generalization problem. They can be mainly divided into four categories: kernel-based methods [32], [33]; domain adversarial learning [34], [35]; explicit feature alignment [36]–[38]; and invariant risk minimization [39], [40]. Explicit feature alignment aims to align the features from source domains to learn domain-invariant representations. For example, Motiian *et al.* [36] developed a cross-domain contrastive loss for representation learning in which mapped domains are semantically matched, while remaining maximally separated. Pan *et al.* [37] implemented Instance Normalization layers to CNNs to improve model generalization. Recently, Fan *et al.* [38] presented that adaptively learning the normalization with the a combination of multiple normalization strategies can improve domain generalization capabilities.

Following the success of self-supervised learning [41], [42]–[44] build self-supervised tasks from the large-scale unlabeled data to learn generalized representations. For instance, Carlucci *et al.* [42] present a self-supervision task of solving jigsaw puzzles to learn the concepts of spatial correlation. Although several self-supervised learning-based domain generalization methods have already achieved promising performance, there is still a significant performance gap for such kinds of methods to attain a desirable result in the specific mammographic image analysis task.

B. Contrastive Learning

Recently, contrastive learning has proven to be quite effective in self-supervised learning. It draws samples from the same class (a positive pair) close together while driving different samples (or negative pairs) apart in the latent embedding space through contrastive loss. Chen *et al.* [45] proposed SimCLR, a contrastive learning-based system for learning effective presentations by maximizing the similarity between the original data image and different, augmented views of it. He *et al.* [46] utilized momentum contrast (MoCo) which divides each image into a query, and then generates a key by performing two distinct augmentations. MoCo v2 [47] incorporates enhancements such as the integration of a two-layer MLP head with ReLU during the unsupervised training stage and the implementation of a data augmentation technique involving blurring. SimCLR and MoCo provided promising

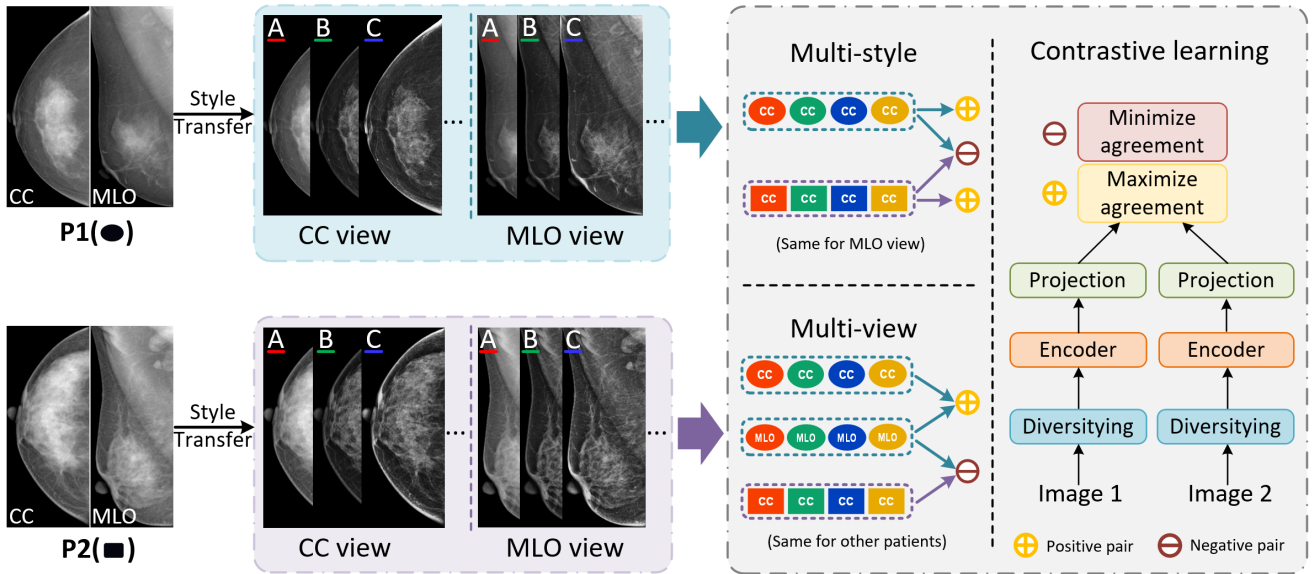


Fig. 3. Illustration of multi-style and multi-view contrastive learning scheme. P1 and P2 indicate different patients. A, B, and C indicate different vendor-style domains, which are generated from one source domain. The red circle with a minus sign inside represents the negative pair, while the yellow circle with a plus sign inside indicates the positive pair. First, the CycleGAN and image blending technique are employed to derive diversified vendor styles. Second, the positive pairs and negative pairs are constructed based on multi-style and multi-view schemes. Finally, contrastive learning is driven by the contrastive loss to maximize the agreement for the positive pairs and minimize the agreement for the negative pairs.

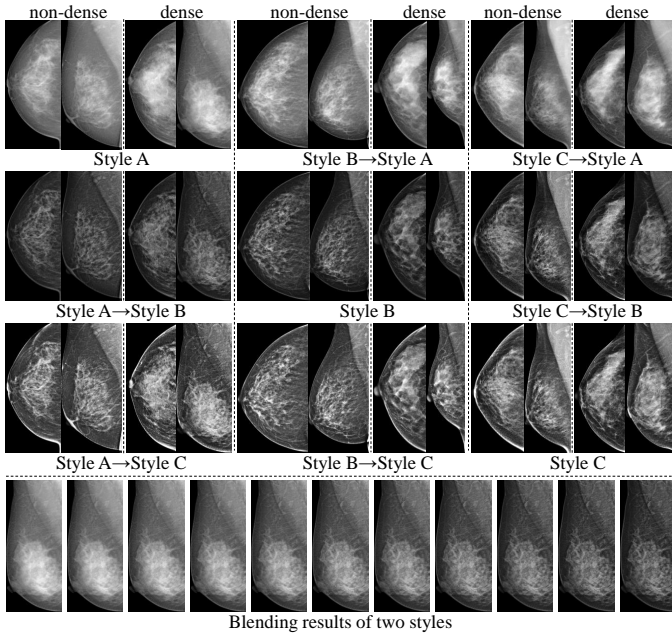


Fig. 4. The first three rows: visual comparison of style transfer results with the CycleGAN for the different vendor domains. Left column: input original images from style A, generated results of style B and style C. Center column: input original images from style B, generated results of style A and style C. Right column: input original images from style C, generated results of style A and style B. A non-dense breast case and a dense breast case are provided for each style. The last row: blending results of style A and style B, with the interpolation factor increasing from 0.0 to 1.0 in increments of 0.1 from left to right.

results which are much closer to supervise-learning compared to other self-supervised learning methods. These frameworks were widely used in the pre-train stage and showed constant improvement for various downstream tasks. Later, Grill et al. [48] introduced a technique called BYOL for learning

feature representations without the massive number of negative pairs. Basically, BYOL added another MLP on the SimCLR to create an asymmetrical architecture. In this paper, we adopt the SimCLR as the pretraining method, because its advantage of easy implementation. Meanwhile, we further replace the SimCLR with both MoCo v2 and BYOL as the pretraining methods. The experimental results suggest there is no significant difference among all pretraining methods.

C. Mammographic Image Analysis

Mass detection is one of the most fundamental problems in mammographic image analysis [5]. Jung et al. [49] use the RetinaNet [50] model as a one-stage mass detector in mammography. Shen et al. [51] proposed a framework that depends on adversarial learning to detect the masses in breast mammograms. The adversarial learning helps align the latent target features from unlabeled datasets with labeled source domain latent features. Moreover, CAD schemes also require supplementary mammographic image analysis functions such as mass matching, malignancy classification, and density classification. Yan et al. [6] exploit multi-tasking properties of deep networks to jointly learn mass matching and classification. Yang et al. [7] present MommiNet-v2 to incorporate the malignant information from both biopsies and BI-RADS categories. Zhao et al. [8] present an innovative bilateral-view adaptive spatial and channel attention network (BASCNet) for fully automated breast density classification. Despite the many existing methods for mammographic image analysis, few of them have been evaluated on unseen domains, which means that their out-of-distribution generalization has not been thoroughly examined.

III. METHOD

Fig. 1 illustrates the proposed domain generalization framework for mammography analysis. Our approach consists of two main stages. In the stage (a), a style-robust backbone is trained with the contrastive learning technique as the pre-trained model for the downstream tasks. To facilitate the contrastive learning, the CycleGAN technique is first employed to diversify the vendor styles. In follows, a multi-style and multi-view contrastive learning scheme is carried to embed a general feature space, which is more robust to both the vendor-style and view domains, in the pre-trained backbone. The common downstream tasks of mammography analysis, which include mass detection, mass matching, BI-RADS rating for mass and breast density classification, are further fine-tuned with the pre-trained backbone for better generalization capability.

A. Contrastive Learning Scheme

Contrastive learning is a self-supervised learning method, which trains a network to encode the image representation into a proper vector space without the need of explicit annotations. The derived model from contrastive learning is commonly served as a pre-trained model to reserve the flexibility for the training and fine-tuning of various downstream tasks.

The basic idea of contrastive learning is to pack the diversified images of the same class/object/subject as positive pairs for the exploration of proper feature embedding. Specifically, given a mini-batch of N images, each example is randomly augmented twice with the diversifying operations, e.g., cropping, rotation, style-transferring, etc., to generate an augmented mini-batch with $2N$ samples. In the augmented mini-batch, two samples from the same image source are treated as a positive pair (i, j) , whereas the other $2(N - 1)$ samples within the mini-batch are regarded as negative pairs. With the positive and negative pairs, contrastive learning is driven by the contrastive loss to maximize the agreement for the positive pairs. The contrastive loss is defined as:

$$\ell_{i,j} = -\log \frac{\exp(\text{sim}(z_i, z_j)/\tau)}{\sum_{k=1}^{2N} \mathbb{1}_{[k \neq i]} \exp(\text{sim}(z_i, z_k)/\tau)}, \quad (1)$$

where $\text{sim}(\cdot)$ is the dot product and z refers to the extracted features. $\mathbb{1}_{[k \neq i]} \in \{0, 1\}$ is an indicator function equaling 1 when $k \neq i$ and τ is a temperature parameter.

By maximizing the agreement for the positive pairs, the learned features of corresponding images are supposed to “attract” each other, while the learned features of non-corresponding images “repel” each other by minimizing the agreement for the negative pairs. We further leverage the concept of contrastive learning to explore the generalization of various vendor styles and the domains of CC and MLO views. The details of multi-style and multi-view contrastive learning are elaborated in the following section.

B. Multi-style and Multi-view Contrastive Learning

To seek the feature embedding with better generalization capability for the vendor-style and view domain, a multi-style and multi-view contrastive learning is devised. The synergy of

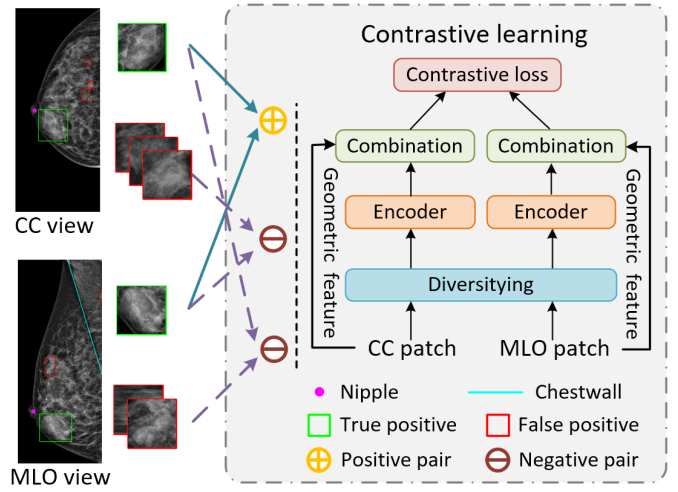


Fig. 5. Illustration of multi-view mass matching contrastive learning scheme. The green boxes indicate true positive mass regions, the red boxes indicate false positive mass regions, the purple dots indicate nipple location and the blue line indicates chestwall.

the two learning scheme is illustrated in Fig. 3. Specifically, we firstly employ CycleGAN to diversify vendor styles of the original data. The style diversifying is further augmented with an image blending operator. Afterward, the positive and negative pairs are further packaged for the contrastive learning in the multi-style and multi-view schemes, respectively. The synergized contrastive learning scheme is further driven with the optimization of both multi-style and -view contrastive losses.

1) *Multi-style Contrastive Learning*: The image styles vary to different vendors and are regarded as distinctive domains. To endow the backbones of downstream tasks with better vendor-style generalization capability, we exploit the CycleGAN [27] and image blending technique as the diversifying operation for contrastive learning. Specifically, given M seen vendor-style domain, we train $\binom{M}{2}$ generators, which map the data distribution of source domain Ω_i to target Ω_j domain, $\forall i, j \in M$. With the $\binom{M}{2}$ generators, each of the original N images in the training set can be diversified into $M - 1$ transferred images, which is illustrated in the first three rows of Fig. 4. Moreover, we further use image blending technique to achieve a smoothly transition between two styles:

$$\text{style}_{blend} = \text{style}_A * (1.0 - \alpha) + \text{style}_B * \alpha \quad (2)$$

where α is the interpolation factor randomly selected from a set of values ranging from 0 to 1 with an interval of 0.1.

In MSCL v2, the two styles of the same source image (e.g. style A and style B from CC view of a patient) are attracted together, while the same view of different patients (e.g. CCs of two patients) are repelled from each other. The positive pairs for contrastive learning are constituted with any two images of the same image source in the original N image set. Therefore, there are possible $N \times \binom{M}{2} \times 11$ positive pairs that be randomly selected in contrastive learning. The contrastive learning is then carried out by minimizing the equation 1 to seek feature embedding space with better generalization capability to various vendor domains.

TABLE II

ABLATION ANALYSIS W.R.T. THE PRE-TRAINING STRATEGY AND OUR METHODS. THE RESULTS ON MAP OF THE MASS DETECTION TASKS ARE REPORTED.

Pretraining Method	Pretraining Dataset	Seen domain				Unseen domain			
		Style A	Style B	Style C	Avg.	Style D	Style E	Style F	Avg.
Random	None	59.8	70.5	66.5	65.6	51.3	79.9	65.8	65.7
Supervised	ImageNet	84.0	85.7	79.1	82.9	82.4	76.3	81.0	79.9
SimCLR	Mammo	84.4	91.6	84.1	86.7	82.2	77.3	75.0	78.2
SimCLR	ImageNet → Mammo	86.9	92.0	86.0	88.3	86.2	80.5	84.2	83.6
MSCL	ImageNet → Mammo	87.6	92.3	85.8	88.6	88.5	85.2	86.0	86.6
MVCL	ImageNet → Mammo	88.9	92.4	84.3	88.5	86.7	85.3	87.3	86.4
MSVCL	ImageNet → Mammo	91.8	94.0	89.1	91.6	87.3	89.7	88.4	88.5
MSCL v2	ImageNet → Mammo	92.2	94.3	86.7	91.1	89.5	86.2	89.0	88.2
MVCL v2	ImageNet → Mammo	90.8	94.1	86.7	90.5	89.7	86.7	90.4	88.9
MSVCL v2	ImageNet → Mammo	92.9	93.8	87.0	91.2	90.4	89.4	94.1	91.3

TABLE III

ABLATION ANALYSIS W.R.T. THE PRE-TRAINING STRATEGY AND OUR METHODS. THE RESULTS ON DOMAIN AVERAGE PERFORMANCE OF FOUR DOWNSTREAM TASKS ARE REPORTED.

Pretraining Method	Pretraining Dataset	Seen domain					Unseen domain				
		Detection	Match	BI-RADS	Density	Avg.	Detection	Match	BI-RADS	Density	Avg.
Random	None	65.6	75.0	55.1	65.3	65.3	65.7	60.3	66.1	40.3	58.1
Supervised	ImageNet	82.9	86.3	85.4	90.3	86.2	79.9	87.4	81.4	77.0	81.4
SimCLR	Mammo	86.7	79.7	79.4	92.3	84.5	78.2	81.5	79.5	73.0	78.1
SimCLR	ImageNet → Mammo	88.3	80.0	87.4	91.7	86.9	83.6	85.0	83.3	76.3	82.1
MSCL	ImageNet → Mammo	88.6	85.7	86.4	91.7	88.1	86.6	87.1	85.8	80.3	85.0
MVCL	ImageNet → Mammo	88.5	89.3	89.2	90.7	89.4	86.4	84.6	84.2	80.3	83.9
MSVCL	ImageNet → Mammo	91.6	89.6	89.3	91.7	90.6	88.5	91.5	85.9	81.0	86.7
MSCL v2	ImageNet → Mammo	91.1	92.0	90.0	93.0	91.5	88.2	89.7	86.8	82.3	86.8
MVCL v2	ImageNet → Mammo	90.5	89.0	87.6	92.3	89.9	88.9	86.9	86.7	82.3	86.2
MSVCL v2	ImageNet → Mammo	91.2	90.6	89.0	92.0	90.7	91.3	92.9	87.8	84.3	89.1

2) *Multi-view Contrastive Learning*: A standard examination of mammography consists of two CC and MLO views. Because the two standard views are mutually complementary, the appearances of CC and MLO images are different. For example, an MLO view includes axilla region, while a CC view doesn't. Accordingly, the domain gap between these two views may exist. To seek view domain-invariant feature embedding for better mammographic image analysis performance, we explore the contrastive learning scheme to consider the distinctive view domains. Specifically, we treat the CC and MLO view of the same breast from the same patient (e.g. LCC and LMLO of a patient) as positive pair, whereas the other combination of the CC and MLO view from different patients (e.g. LCC of patient 1 and LMLO of patient 2) is a negative pair. To further enrich the sample diversity, we further implement style diversifying operations for the CC and MLO in each positive or negative pair. With the prepared sample pairs, MVCL v2 can be carried out for the embedding of view-invariant features.

C. Downstream tasks

1) *Mass Detection*: In this study, we employ the classic single-view detection network of FCOS [52] to identify mass in mammography. The derived pretrained model from the self-supervised learning stage is adopted as the backbone of the FCOS architecture for the realization of the downstream mass detection tasks. Detected results from CC and MLO paired images are two sets of candidate bounding boxes: $B_{cc} = \{b_{cc}^1, \dots, b_{cc}^i, \dots, b_{cc}^N\}$ and $B_{mlo} = \{b_{mlo}^1, \dots, b_{mlo}^j, \dots, b_{mlo}^M\}$.

2) *Mass Matching*: As experts do when making decisions in clinical practice, the underlying concept of mass matching is to simply increase the mass score if a strong match exists in the paired view. For each view, two sets of true-positive (TP) and false-positive (FP) bounding boxes are generated by computing the candidate bounding boxes IoU with the ground truth. We can define them as TP_{cc} , FP_{cc} , TP_{mlo} and FP_{mlo} . Two samples from TP_{cc} and TP_{mlo} whose corresponding ground truths match are treated as a positive pair, and the matching label Y is 1. If one of the samples from FP_{cc} or FP_{mlo} , they are treated as a negative pair, and the matching label Y is 0.

As shown in Fig. 5, the CC/MLO patches matching is based on the similarity of their appearance and geometric features including ROI-to-nipple distance, ROI-to-chestwall distance and ROI size. During training, we choose max margin contrastive loss to calculate the matching error:

$$L_{mat} = \frac{1}{2K} \sum_{k=1}^K Y D^2 + (1 - Y) \max(m - D, 0)^2 \quad (3)$$

where $D = \|f_1 - f_2\|_2$ refers the Euclidean distance between the embedding features of paired samples. The label Y is 1 if the two samples are matched, otherwise 0. The margin m is a hyper-parameter defining the lower bound distance between patches that are not matched.

3) *BI-RADS Classification and Breast Density Classification*: In addition to mass detection and matching, we also evaluate the domain generalization performance of our proposed method on two downstream classification tasks: BI-RADS classification and breast density classification. For BI-RADS

classification, we adopt the pre-trained model to classify each mass into one of the five BI-RADS categories, which include 2~3, 4A, 4B, 4C and 5. In the case of breast density classification, we utilized the pre-trained model to classify breast density into one of the two categories: non-dense and dense.

IV. EXPERIMENTS AND RESULTS

A. Datasets

In this paper, we perform experiments on an in-house dataset and two public datasets. The in-house dataset is collected from four vendors, namely GE, United Imaging Healthcare (UIH), Hologic, and Siemens, which we denote as A, B, C, and D, respectively. All data from four vendors are collected from Asian women. The data from vendors A, B, and C are set as seen domains, while vendor D is treated as an unseen domain. The label information of in-house dataset is first annotated by two radiologists and then reviewed by a senior reader from Beijing Chao-Yang Hospital in China. To evaluate the generalization capability of our method, we also involve two public datasets, INbreast [53] and DDSM [54], denote E and F as the unseen datasets. In total, this study involves 29,700 mammograms (14,850 CC/MLO pairs), where 27,000 unannotated images are used for style transfer and self-supervised learning. The remaining 2,700 annotated images are adopted for the training, validation, and testing of the downstream tasks.

We conduct a preprocessing step to align various mammograms from A, B, C, D, E and F into the consistent pixel spacing of 0.1 mm, to facilitate the training of deep learning methods. A nipple and pectoral muscle segmentation model is applied to each image to calculate the ROI-to-nipple distance and ROI-to-chestwall distance. To quantitatively compare the detector performance, we adopt the mean average precision (mAP) metrics. For the assessment of the other downstream tasks, we adopt the accuracy (acc) metrics.

B. Implementation Details

Our method is developed based on the Pytorch package and trained with NVIDIA Titan RTX GPUs. We train the CycleGAN models with the settings of 50, 100, and 200 epochs, and select the setting (i.e., 100 epochs) that achieved the best mass detection performance on the validation set. The generator backbone consists of ResNet with 9 blocks with 20 convolution layers, while the discriminator is PatchGAN, with six convolution layers for binary classifications. During training, we randomly crop the images to sizes of 512 by 512. MSE and L1 losses are used for classification and reconstruction. For a style transfer, e.g., A to B, the involved training data are both 1000 for balanced training.

We adopt ResNet-50 as the backbone model for contrastive learning and downstream tasks. To ensure fairness in comparison, the learning rate and batch size for all contrastive learning schemes are set the same as 0.3 and 256. Meanwhile, all contrastive learning schemes in all experiments use the same diversifying operations, including random cropping, random

rotation in $\pm 10^\circ$, horizontal flipping and random color jittering (strength=0.2).

The model backbones of downstream tasks are initialized using pre-trained weights from the self-supervised learning stage. For the training of FCOS models, the SGD method is adopted with the parameters of learning rate, weight decay and momentum set as 0.005, 10^{-4} , and 0.9, respectively. The epoch and batch size are set to 50 and 8, respectively, throughout all experiments. Several augmentation methods, e.g. random flipping, scaling, etc., are also implemented during the training of FCOS.

For the training of the other downstream tasks, the SGD method is also adopted with the parameters of learning rate, weight decay and momentum set as 0.001, 10^{-5} , and 0.9, respectively. The epoch and batch size are set to 50 and 128, respectively. In mass matching and BI-RADS classification, the input images are extracted from original mammograms by cropping squares around the center of bounding boxes. The cropping dimension is the long side of the bounding box enlarged by 20% to include useful information around the mass border. For breast density classification, the input images are the original mammograms. All input images are resized to 224*224 pixels, and data augmentation (random flipping, scaling) is implemented synchronously for ipsilaterally paired images. We train matching models with the hyper-parameter margin $m \in \{5, 10, 15\}$ for the contrastive loss (equation 3), and choose $m = 10$.

C. Ablation Study

The ablation experiments are composed of three parts. First, we evaluate the efficacy of original simple contrastive learning (SimCLR) [45] on the downstream tasks. Specifically, we compare downstream tasks performance with 1) no pretraining, 2) ImageNet, 3) SimCLR on Mammo, and 4) SimCLR on ImageNet \rightarrow Mammo pretrained models and report the corresponding performance in the first to fourth rows of Table II and Table III. The third row suggests that SimCLR is trained from scratch with the unlabeled images of vendors A, B and C, where this unlabeled set is denoted as Mammo. The fourth row ImageNet \rightarrow Mammo indicates that SimCLR is initialized with ImageNet parameters and then trained with the Mammo set. In this part, the pretrained model of ImageNet \rightarrow Mammo can yield better overall performance.

The second part is to evaluate the effectiveness of our upgraded version of contrastive learning framework. The results of MSCL v2, MVCL v2 and MSVCL v2 surpass their respective original versions on the unseen domain. We believe the improvements can be attributed to two factors: 1) the increased style diversity enabled better capture of style-invariant features, 2) the more reasonable selection of negative pairs has resulted in superior learning of mammography feature representations.

The third part compares the performance of various MSCL v2, MVCL v2 and MSVCL v2 methods, which are listed in the eighth to tenth rows in Table II and Table III, respectively. The results show that our MSVCL v2 achieves the best result

TABLE IV

PERFORMANCE COMPARISON BETWEEN OUR MSVCL v2 AND OTHER SOTA DOMAIN GENERALIZATION METHODS. THE RESULTS ON MAP OF THE MASS DETECTION TASKS ARE REPORTED.

Method	Seen domain				Unseen domain			
	Style A	Style B	Style C	Avg.	Style D	Style E	Style F	Avg.
Baseline	86.9	92.0	86.0	88.3	86.2	80.5	84.2	83.6
BigAug	88.8	89.9	84.7	87.8	88.4	86.5	84.3	86.4
DD	86.9	90.7	86.1	87.9	87.4	87.9	85.8	87.0
EISNet	89.3	89.1	82.8	87.1	86.2	83.8	85.6	85.2
MSVCL	91.8	94.0	89.1	91.6	87.3	89.7	88.4	88.5
MSVCL v2(ours)	92.9	93.8	87.0	91.2	90.4	89.4	94.1	91.3

TABLE V

PERFORMANCE COMPARISON BETWEEN OUR MSVCL v2 AND OTHER SOTA DOMAIN GENERALIZATION METHODS. THE RESULTS ON DOMAIN AVERAGE PERFORMANCE OF FOUR DOWNSTREAM TASKS ARE REPORTED.

Method	Seen domain					Unseen domain				
	Detection	Match	BI-RADS	Density	Avg.	Detection	Match	BI-RADS	Density	Avg.
Baseline	88.3	88.3	87.4	91.7	88.9	83.6	85.0	83.3	76.3	82.1
BigAug	87.8	88.3	89.0	90.0	88.8	86.4	87.9	83.3	78.7	84.1
DD	87.9	87.9	87.5	90.3	88.4	87.0	88.5	85.3	82.0	85.7
EISNet	87.1	87.1	89.6	88.7	88.1	85.2	90.9	82.4	80.7	84.8
MSVCL	91.6	91.6	89.3	91.7	91.1	88.5	91.5	82.4	81.0	85.9
MSVCL v2(ours)	91.2	91.2	89.3	92.0	90.9	91.3	92.9	87.8	84.3	89.1

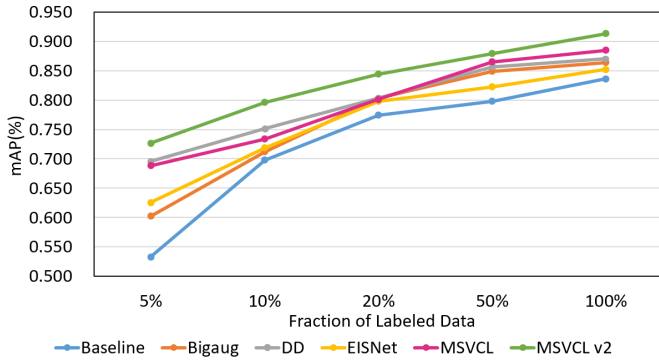


Fig. 6. Performance variation when using different fraction of labeled data during mass detection training. The y-axis is the average mAP (%) of the unseen domain.

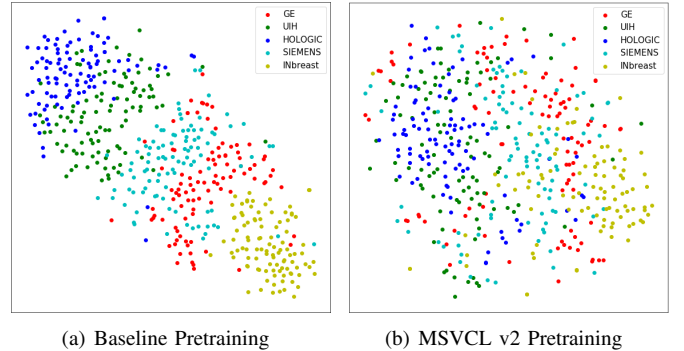


Fig. 7. t-SNE visualization for the pre-trained models from Baseline and MSVCL v2.

on the unseen domain for all downstream tasks. For the seen domain, the MSCL v2 yields the best average performance.

D. Comparison with State-of-the-Art (SOTA) Methods

To further compare with other domain generalization methods, three SOTA methods, i.e., BigAug [29], Domain Diversification (DD) [15], and EISNet [17] are implemented. The BigAug [29] is a conventional data augmentation method, whereas the DD [15] proposed a generative learning method for domain generalization. The EISNet [17] is a learning-based method that explores task-specific and domain-invariant features. Our method on the other hand can decouple the downstream tasks intrinsically and provide task- and domain-invariant features. For a fair comparison, the other methods, including BigAug, DD, and EISNet, were fine-tuned with the pretrained backbone of SimCLR on ImageNet \rightarrow Mammo, to ensure the use of the same amount of data.

The comparison results are shown in Table IV and Table V, where the Baseline row suggests the result of SimCLR with ImageNet \rightarrow Mammo training strategy. As it can be found

in Table V, our MSVCL v2 method achieved the best performance on unseen domains for all downstream tasks. Our method outperformed the BigAug, DD, EISNet and MSVCL by 5.0%, 3.4%, 4.3% and 3.2% respectively, in terms of average downstream tasks performances on unseen domains. For the seen domain, our method outperformed BigAug, DD and EISNet by 2.1%, 2.5%, and 2.7% , while showing comparable performance to MSVCL. Therefore, our method can be a new referential method for the domain generalization of mammographic image analysis task. We also validated five different sizes of the detection training sets: 5%, 10%, 20%, 50%, and 100% label fraction. From Fig. 6, we can observe that our MSVCL v2 obtained the best results across all training label fractions, with the performance gap increasing when the label fraction was small.

To further visually illustrate the efficacy of our MSVCL v2 pretrained model. The t-SNE [55] is employed to visualize the data distribution of various vendor domains in the embedded feature space. Fig. 7 compares the pretrained models of Baseline and MSVCL v2. As can be found, our MSVCL v2 can better break the distribution boundaries between various

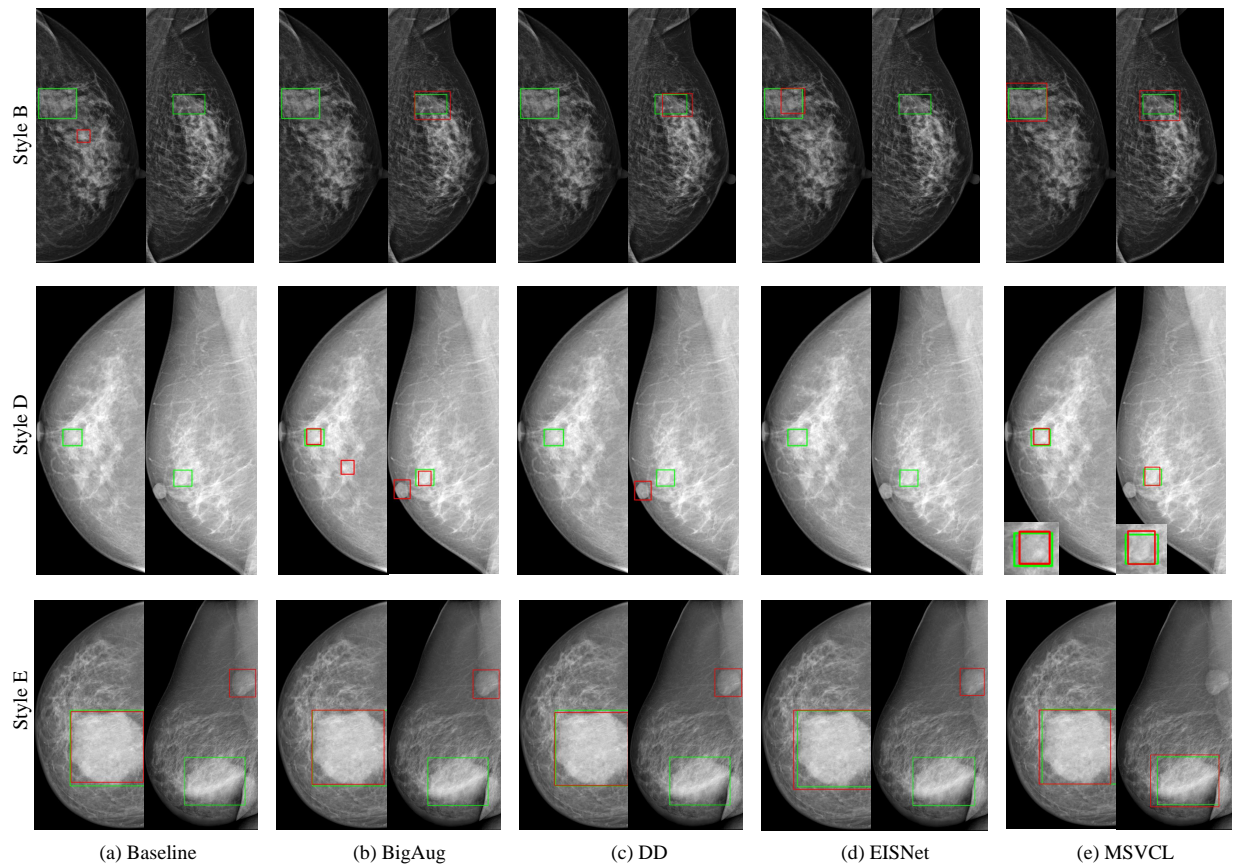


Fig. 8. Qualitative results for mass detection from different methods on one seen domain (style B) and two unseen domains (style D, E). The green boxes refer to the mass regions labeled by the radiologist. The red boxes refer to the mass regions detected by different methods.

vendor domains. Therefore, the encoded features shall be more style-invariant. We also demonstrate the detection results visually in the Fig. 8 for more visual assessment.

V. CONCLUSION AND FUTURE WORK

A novel domain generalization method is proposed to assist the mammographic image analysis tasks. Specifically, we conduct a multi-style and multi-view contrastive learning scheme to embed domain-invariant features in various vendors. Experimental results indicate that our method significantly improves the mammographic image analysis tasks on unseen domains, compared to the four implemented SOTA domain generalization methods. In particular, our method achieves the best performance on public datasets INbreast and DDSM, which belong to not only unseen domains but also different populations, further corroborating its efficacy. Furthermore, the visualization outcomes demonstrate that our proposed method offers realistic and understandable visual clues for the clinical diagnosis.

Future work will include: (1) verifying the effectiveness of our method on the transformer backbone; (2) exploring more powerful implementations of self-supervised learning techniques; (3) integrating bilateral (same view of the left and right breasts) domain knowledge of mammography into our scheme.

REFERENCES

- [1] R. L. Siegel, K. D. Miller, H. E. Fuchs, and A. Jemal, "Cancer statistics, 2022," *CA: a cancer journal for clinicians*, vol. 72, no. 1, pp. 7–33, 2022.
- [2] W. Lotter, A. R. Diab, B. Haslam, J. G. Kim, G. Grisot, E. Wu, K. Wu, J. O. Onieva, Y. Boyer, J. L. Boxerman *et al.*, "Robust breast cancer detection in mammography and digital breast tomosynthesis using an annotation-efficient deep learning approach," *Nature Medicine*, pp. 1–6, 2021.
- [3] S. M. McKinney, M. Sieniek, V. Godbole, J. Godwin, N. Antropova, H. Ashrafiyan, T. Back, M. Chesus, G. C. Corrado, A. Darzi *et al.*, "International evaluation of an ai system for breast cancer screening," *Nature*, vol. 577, no. 7788, pp. 89–94, 2020.
- [4] M. Salim, E. Wählén, K. Dembrower, E. Azavedo, T. Foukakis, Y. Liu, K. Smith, M. Eklund, and F. Strand, "External evaluation of 3 commercial artificial intelligence algorithms for independent assessment of screening mammograms," *JAMA oncology*, vol. 6, no. 10, pp. 1581–1588, 2020.
- [5] L. Abdelrahman, M. Al Ghamdi, F. Collado-Mesa, and M. Abdel-Mottaleb, "Convolutional neural networks for breast cancer detection in mammography: A survey," *Computers in biology and medicine*, vol. 131, p. 104248, 2021.
- [6] Y. Yan, P.-H. Conze, M. Lamard, G. Quellec, B. Cochener, and G. Coatrieux, "Towards improved breast mass detection using dual-view mammogram matching," *Medical Image Analysis*, vol. 71, p. 102083, 2021.
- [7] Z. Yang, Z. Cao, Y. Zhang, Y. Tang, X. Lin, R. Ouyang, M. Wu, M. Han, J. Xiao, L. Huang *et al.*, "Momminet-v2: Mammographic multi-view mass identification networks," *Medical Image Analysis*, vol. 73, p. 102204, 2021.
- [8] W. Zhao, R. Wang, Y. Qi, M. Lou, Y. Wang, Y. Yang, X. Deng, and Y. Ma, "Bascnet: Bilateral adaptive spatial and channel attention network for breast density classification in the mammogram," *Biomedical Signal Processing and Control*, vol. 70, p. 103073, 2021. [Online]. Available: <https://www.sciencedirect.com/science/article/pii/S1746809421006704>

- [9] L. Garrucho, K. Kushibar, S. Jouide, O. Diaz, L. Igual, and K. Lekadir, "Domain generalization in deep learning based mass detection in mammography: A large-scale multi-center study," *Artificial Intelligence in Medicine*, vol. 132, p. 102386, 2022.
- [10] X. Liu, B. Glocker, M. M. McCradden, M. Ghassemi, A. K. Denniston, and L. Oakden-Rayner, "The medical algorithmic audit," *The Lancet Digital Health*, 2022.
- [11] E. Romera, L. M. Bergasa, J. M. Alvarez, and M. Trivedi, "Train here, deploy there: Robust segmentation in unseen domains," in *2018 IEEE Intelligent Vehicles Symposium (IV)*. IEEE, 2018, pp. 1828–1833.
- [12] R. Volpi, H. Namkoong, O. Sener, J. C. Duchi, V. Murino, and S. Savarese, "Generalizing to unseen domains via adversarial data augmentation," in *NeurIPS*, 2018.
- [13] X. Yue, Y. Zhang, S. Zhao, A. Sangiovanni-Vincentelli, K. Keutzer, and B. Gong, "Domain randomization and pyramid consistency: Simulation-to-real generalization without accessing target domain data," in *Proceedings of the IEEE/CVF International Conference on Computer Vision*, 2019, pp. 2100–2110.
- [14] S. Wang, J. Huo, X. Ouyang, J. Che, Z. Xue, D. Shen, Q. Wang, and J.-Z. Cheng, "mr2nst: Multi-resolution and multi-reference neural style transfer for mammography," in *International Workshop on Predictive Intelligence In Medicine*. Springer, 2020, pp. 169–177.
- [15] T. Kim, M. Jeong, S. Kim, S. Choi, and C. Kim, "Diversify and match: A domain adaptive representation learning paradigm for object detection," in *Proceedings of the IEEE/CVF Conference on Computer Vision and Pattern Recognition*, 2019, pp. 12456–12465.
- [16] S. Zakharov, W. Kehl, and S. Ilic, "Deceptionnet: Network-driven domain randomization," in *Proceedings of the IEEE/CVF International Conference on Computer Vision*, 2019, pp. 532–541.
- [17] S. Wang, L. Yu, C. Li, C.-W. Fu, and P.-A. Heng, "Learning from extrinsic and intrinsic supervisions for domain generalization," in *European Conference on Computer Vision*. Springer, 2020, pp. 159–176.
- [18] Q. Liu, Q. Dou, and P.-A. Heng, "Shape-aware meta-learning for generalizing prostate mri segmentation to unseen domains," in *International Conference on Medical Image Computing and Computer-Assisted Intervention*. Springer, 2020, pp. 475–485.
- [19] Q. Dou, D. C. Castro, K. Kamnitsas, and B. Glocker, "Domain generalization via model-agnostic learning of semantic features," *arXiv preprint arXiv:1910.13580*, 2019.
- [20] H. Li, S. J. Pan, S. Wang, and A. C. Kot, "Domain generalization with adversarial feature learning," in *Proceedings of the IEEE Conference on Computer Vision and Pattern Recognition*, 2018, pp. 5400–5409.
- [21] Y. Li, X. Tian, M. Gong, Y. Liu, T. Liu, K. Zhang, and D. Tao, "Deep domain generalization via conditional invariant adversarial networks," in *Proceedings of the European Conference on Computer Vision (ECCV)*, 2018, pp. 624–639.
- [22] Z. Cui, C. Li, Z. Du, N. Chen, G. Wei, R. Chena, L. Yang, D. Shen, and W. Wang, "Structure-driven unsupervised domain adaptation for cross-modality cardiac segmentation," *IEEE Transactions on Medical Imaging*, 2021.
- [23] N. Chen, L. Liu, Z. Cui, R. Chen, D. Ceylan, C. Tu, and W. Wang, "Unsupervised learning of intrinsic structural representation points," in *Proceedings of the IEEE/CVF Conference on Computer Vision and Pattern Recognition*, 2020, pp. 9121–9130.
- [24] S. Azizi, B. Mustafa, F. Ryan, Z. Beaver, J. Freyberg, J. Deaton, A. Loh, A. Karthikesalingam, S. Kornblith, T. Chen *et al.*, "Big self-supervised models advance medical image classification," *arXiv preprint arXiv:2101.05224*, 2021.
- [25] H. Sowrirajan, J. Yang, A. Y. Ng, and P. Rajpurkar, "Moco pretraining improves representation and transferability of chest x-ray models," *arXiv preprint arXiv:2010.05352*, 2020.
- [26] H.-Y. Zhou, S. Yu, C. Bian, Y. Hu, K. Ma, and Y. Zheng, "Comparing to learn: Surpassing imagenet pretraining on radiographs by comparing image representations," in *International Conference on Medical Image Computing and Computer-Assisted Intervention*. Springer, 2020, pp. 398–407.
- [27] J.-Y. Zhu, T. Park, P. Isola, and A. A. Efros, "Unpaired image-to-image translation using cycle-consistent adversarial networks," in *Proceedings of the IEEE international conference on computer vision*, 2017, pp. 2223–2232.
- [28] Z. Li, Z. Cui, S. Wang, Y. Qi, X. Ouyang, Q. Chen, Y. Yang, Z. Xue, D. Shen, and J.-Z. Cheng, "Domain generalization for mammography detection via multi-style and multi-view contrastive learning," in *International Conference on Medical Image Computing and Computer-Assisted Intervention*. Springer, 2021, pp. 98–108.
- [29] L. Zhang, X. Wang, D. Yang, T. Sanford, S. Harmon, B. Turkbey, B. J. Wood, H. Roth, A. Myronenko, D. Xu *et al.*, "Generalizing deep learning for medical image segmentation to unseen domains via deep stacked transformation," *IEEE transactions on medical imaging*, vol. 39, no. 7, pp. 2531–2540, 2020.
- [30] D. Mahajan, S. Tople, and A. Sharma, "Domain generalization using causal matching," in *International Conference on Machine Learning*. PMLR, 2021, pp. 7313–7324.
- [31] X. Li, W. Zhang, H. Ma, Z. Luo, and X. Li, "Domain generalization in rotating machinery fault diagnostics using deep neural networks," *Neurocomputing*, vol. 403, pp. 409–420, 2020.
- [32] G. Blanchard, A. A. Deshmukh, U. Dogan, G. Lee, and C. Scott, "Domain generalization by marginal transfer learning," *Journal of machine learning research*, 2021.
- [33] S. Hu, K. Zhang, Z. Chen, and L. Chan, "Domain generalization via multidomain discriminant analysis," in *Uncertainty in Artificial Intelligence*. PMLR, 2020, pp. 292–302.
- [34] R. Gong, W. Li, Y. Chen, and L. V. Gool, "Dlow: Domain flow for adaptation and generalization," in *Proceedings of the IEEE/CVF conference on computer vision and pattern recognition*, 2019, pp. 2477–2486.
- [35] S. Zhao, M. Gong, T. Liu, H. Fu, and D. Tao, "Domain generalization via entropy regularization," *Advances in Neural Information Processing Systems*, vol. 33, pp. 16096–16107, 2020.
- [36] S. Motiian, M. Piccirilli, D. A. Adjeroh, and G. Doretto, "Unified deep supervised domain adaptation and generalization," in *Proceedings of the IEEE international conference on computer vision*, 2017, pp. 5715–5725.
- [37] X. Pan, P. Luo, J. Shi, and X. Tang, "Two at once: Enhancing learning and generalization capacities via ibn-net," in *Proceedings of the European Conference on Computer Vision (ECCV)*, 2018, pp. 464–479.
- [38] X. Fan, Q. Wang, J. Ke, F. Yang, B. Gong, and M. Zhou, "Adversarially adaptive normalization for single domain generalization," in *Proceedings of the IEEE/CVF Conference on Computer Vision and Pattern Recognition*, 2021, pp. 8208–8217.
- [39] K. Ahuja, E. Caballero, D. Zhang, J.-C. Gagnon-Audet, Y. Bengio, I. Mitliagkas, and I. Rish, "Invariance principle meets information bottleneck for out-of-distribution generalization," *Advances in Neural Information Processing Systems*, vol. 34, 2021.
- [40] D. Krueger, E. Caballero, J.-H. Jacobsen, A. Zhang, J. Binas, D. Zhang, R. Le Priol, and A. Courville, "Out-of-distribution generalization via risk extrapolation (rex)," in *International Conference on Machine Learning*. PMLR, 2021, pp. 5815–5826.
- [41] L. Jing and Y. Tian, "Self-supervised visual feature learning with deep neural networks: A survey," *IEEE transactions on pattern analysis and machine intelligence*, vol. 43, no. 11, pp. 4037–4058, 2020.
- [42] F. M. Carlucci, A. D'Innocente, S. Bucci, B. Caputo, and T. Tommasi, "Domain generalization by solving jigsaw puzzles," in *Proceedings of the IEEE/CVF Conference on Computer Vision and Pattern Recognition*, 2019, pp. 2229–2238.
- [43] D. Kim, Y. Yoo, S. Park, J. Kim, and J. Lee, "Selfreg: Self-supervised contrastive regularization for domain generalization," in *Proceedings of the IEEE/CVF International Conference on Computer Vision*, 2021, pp. 9619–9628.
- [44] S. Jeon, K. Hong, P. Lee, J. Lee, and H. Byun, "Feature stylization and domain-aware contrastive learning for domain generalization," in *Proceedings of the 29th ACM International Conference on Multimedia*, 2021, pp. 22–31.
- [45] T. Chen, S. Kornblith, M. Norouzi, and G. Hinton, "A simple framework for contrastive learning of visual representations," in *International conference on machine learning*. PMLR, 2020, pp. 1597–1607.
- [46] K. He, H. Fan, Y. Wu, S. Xie, and R. Girshick, "Momentum contrast for unsupervised visual representation learning," in *Proceedings of the IEEE/CVF conference on computer vision and pattern recognition*, 2020, pp. 9729–9738.
- [47] X. Chen, H. Fan, R. Girshick, and K. He, "Improved baselines with momentum contrastive learning," *arXiv preprint arXiv:2003.04297*, 2020.
- [48] J.-B. Grill, F. Strub, F. Alché, C. Tallec, P. Richemond, E. Buchatskaya, C. Doersch, B. Avila Pires, Z. Guo, M. Gheshlaghi Azar *et al.*, "Bootstrap your own latent—a new approach to self-supervised learning," *Advances in Neural Information Processing Systems*, vol. 33, pp. 21271–21284, 2020.
- [49] H. Jung, B. Kim, I. Lee, M. Yoo, J. Lee, S. Ham, O. Woo, and J. Kang, "Detection of masses in mammograms using a one-stage object detector based on a deep convolutional neural network," *PLoS one*, vol. 13, no. 9, p. e0203355, 2018.
- [50] T.-Y. Lin, P. Goyal, R. Girshick, K. He, and P. Dollár, "Focal loss for dense object detection," in *Proceedings of the IEEE international conference on computer vision*, 2017, pp. 2980–2988.

- [51] R. Shen, J. Yao, K. Yan, K. Tian, C. Jiang, and K. Zhou, "Unsupervised domain adaptation with adversarial learning for mass detection in mammogram," *Neurocomputing*, vol. 393, pp. 27–37, 2020.
- [52] Z. Tian, C. Shen, H. Chen, and T. He, "Fcos: Fully convolutional one-stage object detection," in *Proceedings of the IEEE/CVF International Conference on Computer Vision*, 2019, pp. 9627–9636.
- [53] I. C. Moreira, I. Amaral, I. Domingues, A. Cardoso, M. J. Cardoso, and J. S. Cardoso, "Inbreast: toward a full-field digital mammographic database," *Academic radiology*, vol. 19, no. 2, pp. 236–248, 2012.
- [54] M. Heath, K. Bowyer, D. Kopans, R. Moore, and W. Kegelmeyer, "The digital database for screening mammography," *Proceedings of the 5th international workshop on digital mammography*, pp. 212–218, 2000.
- [55] L. Van der Maaten and G. Hinton, "Visualizing data using t-sne." *Journal of machine learning research*, vol. 9, no. 11, 2008.